Engineering Fracture Mechanics 289 (2023) 109435

Contents lists available at ScienceDirect

Engineering Fracture Mechanics

journal homepage: www.elsevier.com/locate/engfracmech

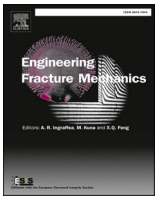

Inelastic zone around crack tip in polyacrylamide hydrogel identified using digital image correlation

Yudong Pan [a], Yifan Zhou [a], Zhigang Suo [b,*], Tongqing Lu [a,*]

[a] State Key Lab for Strength and Vibration of Mechanical Structures, Soft Machines Lab, International Center for Applied Mechanics, Department of Engineering Mechanics, Xi'an Jiaotong University, Xi'an 710049, China
[b] John A. Paulson School of Engineering and Applied Sciences, Kavli Institute for Bionano Science and Technology, Harvard University, MA 02138, USA

ARTICLE INFO

Keywords:
Inelastic zone
G-annulus
Polyacrylamide hydrogel
Digital image correlation

ABSTRACT

Prior to fracture, a polyacrylamide hydrogel has a stress-stretch curve of nearly perfect elasticity, but it has been suggested that an inelastic zone exists around a crack tip. This inelastic zone, however, has never been observed directly in a polyacrylamide hydrogel. Here we identify the inelastic zone using digital image correlation (DIC). We prepare a polyacrylamide hydrogel with a precut crack. While a sample of the hydrogel is stretched, the speckle patterns are recorded using a microscope or a camera, with pixel size 2.3 μm and 22.7 μm, respectively. The speckle patterns recorded by the microscope and camera are processed using the DIC software, and merged to provide the deformation field over the entire sample. The measured field of deformation is used to calculate the field of energy density according to the neo-Hookean model. When the body is perfectly elastic, the field of energy density around the crack tip is inversely proportional to the distance from the crack tip. The difference between the measured field and the predicted elastic field identifies the inelastic zone. The measured size of the inelastic zone is ~ 0.6 mm. We further confirm that, when a sample is much larger than the inelastic zone, an annulus exists, in which the elastic crack tip field prevails.

1. Introduction

A hydrogel is an aggregate of a polymer network and water. Water has low viscosity and lubricates polymer chains. For a polyacrylamide hydrogel, the physical association between polymer chains is weak, so that the stress-stretch curve exhibits nearly perfect elasticity [1–3]. Despite the near-perfect elasticity, it has been suggested that an inelastic zone exists around a crack tip for a polyacrylamide hydrogel containing a precut crack. This inelastic zone, however, has never been observed directly in a polyacrylamide hydrogel.

In this work, we use the digital image correlation (DIC) to identify the inelastic zone around a crack tip in a polyacrylamide hydrogel. We use a microscope with the spatial resolution of 2.3 μm per pixel to observe the field near the crack tip, and use a camera with the spatial resolution of 22.7 μm per pixel to observe the field over a larger scale. The speckle patterns recorded by the microscope and camera are processed using the DIC software, and merged to provide the deformation field over the entire sample. The field of energy density is calculated using the measured deformation field. When the body is perfectly elastic, the field of energy density

* Corresponding authors.
E-mail addresses: suo@seas.harvard.edu (Z. Suo), tongqinglu@mail.xjtu.edu.cn (T. Lu).

https://doi.org/10.1016/j.engfracmech.2023.109435
Received 22 March 2023; Received in revised form 14 June 2023; Accepted 14 June 2023
Available online 20 June 2023

around the crack tip is inversely proportional to the distance from the crack tip. For the material particles distant from the crack tip, the deformation field agrees with the elastic solution. For the material particles close to the crack tip, the deformation may deviate from the elastic solution, which identifies the size of the inelastic zone. The measured size of the inelastic zone is ~ ~~0.5~~ 0.6 mm. We further show that, when a sample is much larger than the inelastic zone, an annulus exists, in which the elastic crack tip field prevails.

Crack tip field has been observed by DIC in various materials before. The crack tip field of metal under cyclic loads has been observed and the plastic zone around the crack tip was identified by the residual strain after unloading [4,5]. The crack tip field of polyacrylamide/Ca-alginate hydrogel has been observed and compared with the prediction of the proposed constitutive model. In this case, the entire sample undergoes inelastic deformation [6]. The crack tip field of a carbon-filled elastomer has been observed and the size of the process zone is determined by selecting the strain level 0.9 times of the maximum strain measured at crack tip [7]. The crack tip deformation of Ecoflex has been observed and compared with asymptotic elastic solution of crack tip field, but the inelastic zone close to the crack tip was not observed, possibly due to low resolution [8]. The crack tip field can also be observed using photoelasticity [9,10], light scattering [8], and chemiluminescent crosslinker [11].

2. *G*-annulus

2.1. Elastic crack tip field

In the literature, by an elastic crack tip field it means a field for a semi-infinite crack in an infinite elastic body. The elastic crack tip field is commonly determined by asymptotic analysis. The field depends on the constitutive model of elasticity. Examples include linear elasticity [12], materials of power-law stress–strain relations [13,14], and neo-Hookean material [15].

Here we focus on a result common to elastic crack tip fields in materials of any constitutive model of elasticity. Consider a semi-infinite crack in an infinite elastic body. When the body is in the undeformed state, label a material particle by polar coordinates (R, Θ) centered at the tip of the crack (Fig. 1a). We will report each material particle using its coordinates when the body is in the undeformed state. When the body is in a deformed state, the same material particle moves to a different place in space (Fig. 1b). Represent the applied load by energy release rate G. In the deformed state, the elastic field is a field of the coordinates of material particles in the undeformed state. In particular, the field of energy density is a function $W(R, \Theta)$. For any constitutive model of elasticity, the field of energy density scales with the energy release rate as

$$W(R,\Theta) = \frac{G}{R} f(\Theta) \tag{1}$$

Here f is a dimensionless function of the polar angle Θ, and is independent of R. This scaling relation is understood from dimensional considerations. The field of energy density, W, has the dimension of energy per unit volume. The energy release rate, G, has the dimension of energy per unit area. The equations that govern elastic fields have no length scale. For a semi-infinite crack in an infinite elastic body, the boundary conditions also provide no length scale. For each material particle, the only length scale is the distance R of the material particle from the crack tip. Consequently, the field of energy density scales with the energy release rate as $W \sim G/R$.

The scaling relation (1) obtained from the dimensional considerations is independent of constitutive models of elasticity, and is valid for both linear elasticity and nonlinear elasticity. For example, when the material is linearly elastic, the energy density is quadratic in stress, so that the stress field at a crack tip is square-root singular, which is a well-known result. For an elastic material of power law stress–strain relation, the scaling relation (1) is also obtained, and is commonly justified on the basis of the J integral [13,14,16]. For nonlinear elastic material, the scaling relation (1) is confirmed by the crack tip fields solved by asymptotic analysis [17,18].

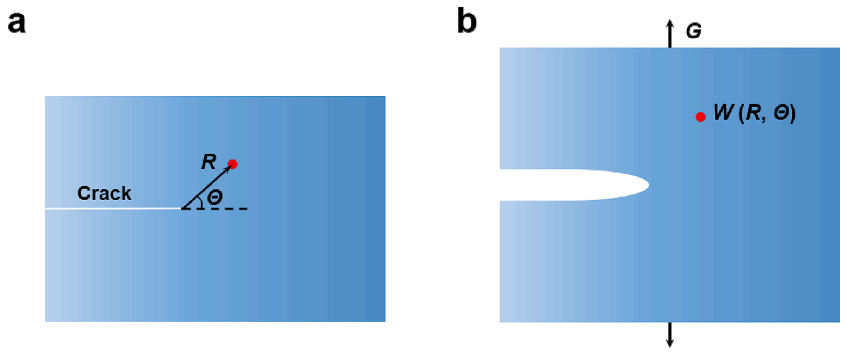

Fig. 1. A semi-infinite crack in an infinite elastic body. (a) In the undeformed state, a material particle is labeled by polar coordinates (R, Θ) centered at the tip of the crack. (b) In the deformed state, the applied load is represented by the energy release rate G. The field of energy density is a function $W(R, \Theta)$.

2.2. G-annulus

A real body containing a crack and subject to a load is finite in size and undergoes inelastic deformation at the crack tip. In the undeformed state, label a material particle in the sample by polar coordinates (R, Θ) centered at the tip of the crack (Fig. 2a). In the undeformed state, denote the length of the crack by C, and a length representative of sample size by H. In the deformed state, the same material particle moves to a different place in space (Fig. 2b). In the deformed state, an inelastic zone forms around the crack tip, while the remaining material is elastic. We denote the size of the inelastic zone by R_1 in the undeformed state. The body undergoes small-scale inelasticity when the inelastic zone is much smaller than the crack length and sample size, $R_1 \ll C$, and $R_1 \ll H$. Under the condition of small-scale inelasticity, a G-annulus exists, $R_1 < R < R_2$. The inner radius R_1 is the boundary of the inelastic zone, and the outer radius R_2 is a fraction of the crack length or sample size. Within the G-annulus, the deformation field is the same as that of a semi-infinite crack in an infinite elastic body. The elastic crack tip field (1) is invalid outside the G-annulus. When $R < R_1$, the field in the body is affected by inelasticity. When $R > R_2$, the field in the body is affected by the external boundary (Fig. 2c).

3. Experiments

3.1. Chemical synthesis and mechanical tests

We synthesize a polyacrylamide hydrogel as follows. The monomer acrylamide (AAm; Aladdin, A108465) (7 g) and crosslinker N, N'-Methylenebisacrylamide (MBAA; Aladdin, M104022) (0.0152 g) are dissolved in deionized water (43 g). The photo-initiator 2-Hydroxy-4′-(2-hydroxyethoxy)-2-methylpropiophenone (Irgacure 2959, Aladdin, H137984) is dissolved in ethyl alcohol to form a solution of concentration of 0.1 M. For every 1 ml of the solution of the monomer and crosslinker, 4.6 μl of the solution of initiator is added. All chemicals are purchased and used without further purification. The solution is poured into a reaction vessel made of two parallel glass sheets separated by a 1 mm thick silicone spacer, and cured under the 365 nm UV light with intensity of 5.5 mW/cm^2 for 2 h. After cure, we disassemble the mold and obtain the polyacrylamide hydrogel.

We use the uniaxial tension test to measure the stress-stretch curve of the polyacrylamide hydrogel. The hydrogel is punctured into dumbbell-shaped samples with 25 mm in width and 150 mm in gauge length.

We prepare a long rectangular sample with a long precut. The sample is then clamped along the two long edges, and pulled and stretched in the pure-shear configuration [19]. The samples are punctured into rectangular samples with a long crack, and then glue the samples onto PMMA (polymethyl methacrylate) sheets with cyanoacrylate. The samples of the hydrogel are 1 mm thick, 50 mm long, and 10 mm high. The crack is 20 mm long. The uniaxial tension tests and pure shear tests were performed on a tensile machine (SHIMADZU AGS-X) with a velocity of 0.01 s^{-1}.

3.2. The stress-stretch curves and hysteresis under uniaxial tension

Fig. 3a shows the stress-stretch curves of polyacrylamide hydrogel under uniaxial tension. The samples are loaded until fracture. The tests are repeated five times. The curves are fit to incompressible neo-Hookean model, with the energy density function as:

$$W = \frac{\mu}{2}\left(\lambda_1^2 + \lambda_2^2 + \lambda_1^{-2}\lambda_2^{-2} - 3\right) \tag{2}$$

where μ is the shear modulus, λ_1, λ_2 are the in-plane principal stretches. The hydrogel is taken to be incompressible, so that the out-of-plane stretch λ_3 is calculated by $(\lambda_1\lambda_2)^{-1}$. The load is applied along direction 2. The nominal stress is calculated from $s_2 - s_3/\left(\lambda_1\lambda_2^2\right) = \partial W/\partial\lambda_2$. For uniaxial tension, $s_2 = s$, $s_3 = 0$, $\lambda_2 = \lambda$, $\lambda_1 = \lambda^{-1/2}$, we have

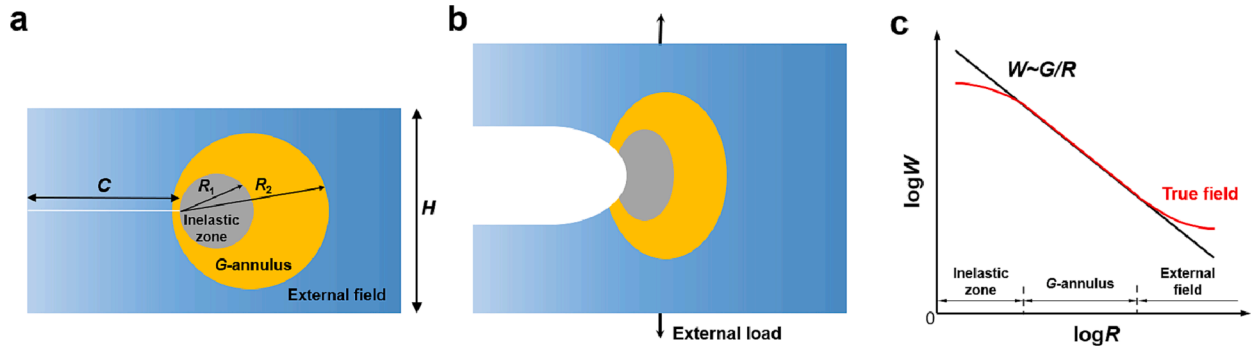

Fig. 2. A body containing a crack and subject to a load. (a) Undeformed state. Three regions are divided: inelastic zone, G-annulus, and external field. (b) Deformed state. (c) The field of energy density, W (R, Θ), is plotted as a function of R for a fixed Θ. The line, $W \sim G/R$, represents the field around a semi-infinite crack in an infinite elastic body. The true field in the actual sample coincides with $W \sim G/R$ within the G-annulus, but deviates from $W \sim G/R$ outside the G-annulus.

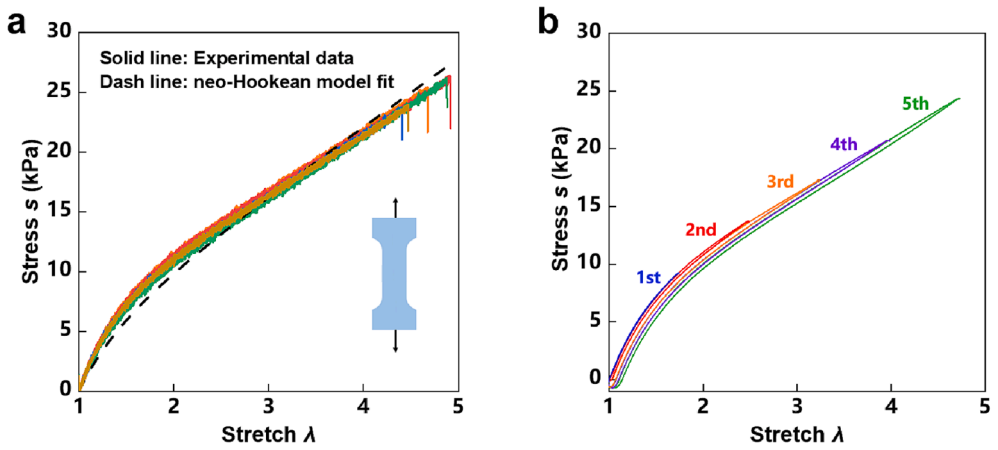

Fig. 3. (a) Stress-stretch curves of uniaxial tension of a polyacrylamide hydrogel. The test is repeated five times. The Neo-Hookean model is fit to experimental data (the fitted shear modulus is $\mu = 5.614$ kPa). (b) A sample is subject to loading, unloading, and reloading.

$$s = \mu\left(\lambda - \lambda^{-2}\right) \tag{3}$$

The dashed fitting curve gives the fitting parameter $\mu = 5.614$ kPa (Fig. 3a).

We load, unload, and reload a sample to a sequence of maximum stretches (Fig. 3b). When the stretch is less than the previous stretch, the reloading curve is only slightly below the previous loading curve. When the stretch is larger than the previous stretch, the

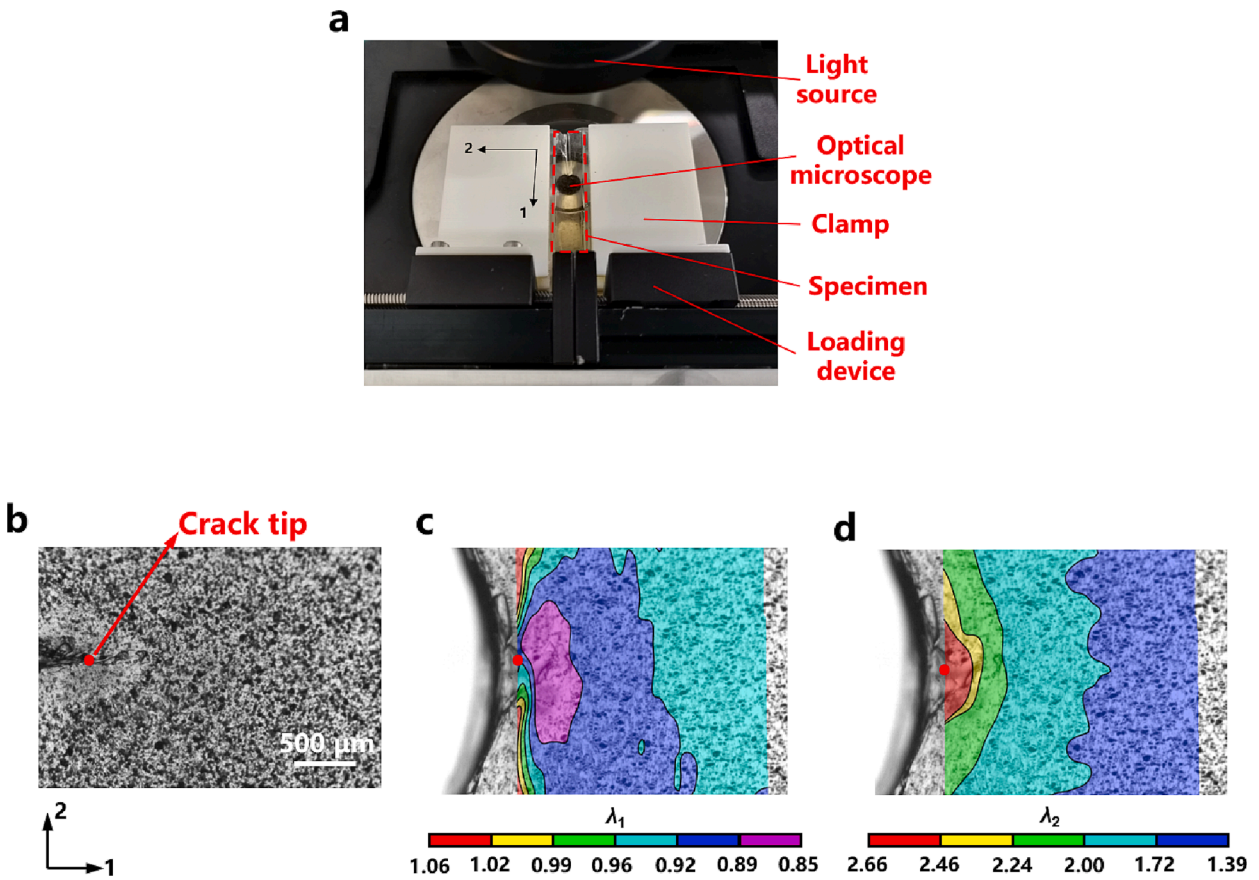

Fig. 4. Observe deformation field using the DIC method with a high resolution. (a) The sample is loaded on a test platform, observed by an optical microscope with a resolution of 2.3 μm/pixel. The sample is subject to an applied stretch of $\lambda_{\text{appl}} = 1.62$. (b) Speckle patterns of the sample in the undeformed state. (c) Contours of principal stretch λ_1. (d) Contours of principal stretch λ_2.

stress–stretch curve is approximately the same as if the sample has not been previously stretched. These observations confirm the near-perfect elasticity of the polyacrylamide hydrogel.

3.3. Measure crack tip field using digital image correlation

Digital image correlation is a non-contact optical technique that allows full-field strain measurement on a surface under deformation [20]. We spray the black paint on the surface of hydrogel samples using an airbrush to obtain a fine speckle pattern. Images of speckle patterns at the undeformed state and all the subsequent deformed states are recorded. We use two testing systems with different resolutions to record the images. The first system uses a homemade tension device to stretch the sample and an optical microscope (SOPTOP XD) with spatial resolution of 2.3 μm/pixel to record the images (Fig. 4a). The second system uses the tensile machine (SHIMADZU AGS-X) to stretch the sample and a CCD (charge coupled device) video camera with spatial resolution of 22.7 μm/pixel to record the images (Fig. 5a). The first system is used to observe the field very close to the crack tip and the second system is used to observe the field on the scale of the sample.

The images obtained from the above two systems are transformed to gray scale images. To track the displacements of the surface particles during deformation, a mathematically well-defined correlated function r(x, y) is applied to match digitized images before deformation and after deformation [21]

$$r(x,y) = 1 - \frac{\sum A(x,y)B(x^*,y^*)}{(\sum A(x,y)^2 * \sum B(x^*,y^*)^2)^{1/2}} \tag{4}$$

where $A(x, y)$ is the gray level at the location of (x, y) at reference state, $B(x^*, y^*)$ represents the gray level at the location of (x^*, y^*) at deformed state. The relation between (x^*, y^*) and (x, y) is:

$$\begin{cases} x^* = x + u + \dfrac{\partial u}{\partial x}\Delta x + \dfrac{\partial u}{\partial y}\Delta y \\ y^* = y + v + \dfrac{\partial v}{\partial x}\Delta x + \dfrac{\partial v}{\partial y}\Delta y \end{cases} \tag{5}$$

where u and v respectively represent the displacements in the direction of x and y. The displacements can be determined by minimizing the correlated function $r(x, y)$. The in-plane strain field of the undeformed state and deformed state are analyzed via VIC-2D software. The incremental correlation is set to account for the large deformation of samples. In this case, each image is computed relative to the previous one, not relative to the reference image.

When the sample is stretched, the crack blunts and grows. The process of growth is too fast to capture, so we select the image near the onset of growth. Fig. 4b shows the speckle patterns at the undeformed state and Fig. 4c, d show the in-plane stretch field contours (λ_1, λ_2) at the applied stretch 1.62 observed using the microscope. Fig. 5b, c, d shows the deformation field of another sample at the applied stretch 1.62 observed using the camera.

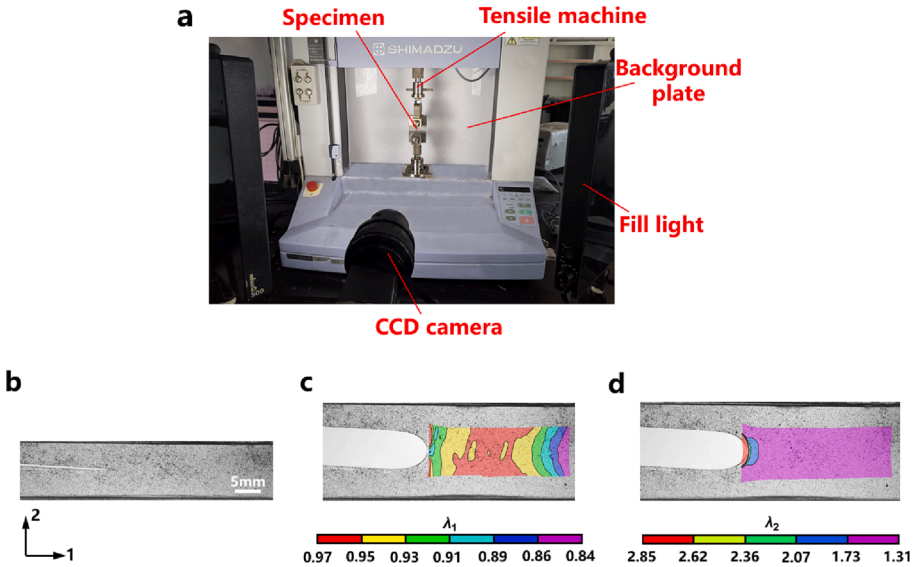

Fig. 5. Observe deformation field using the DIC method with a low resolution. (a) The sample is loaded on a tensile tester, observed by a camera with a resolution of 22.7 μm/pixel. The sample is subject to an applied stretch of $\lambda_{appl} = 1.62$. (b) Speckle patterns of the sample in the undeformed state. (c) Contours of principal stretch λ_1. (d) Contours of principal stretch λ_2.

4. Results and discussion

Fig. 6 shows the observed in-plane stretches (λ_1, λ_2) as a function of distance from the crack tip at the applied stretches $\lambda_{appl} = 1.62$. The data observed by the optical microscope with a high resolution is marked by blue, and the data observed by the camera with a low resolution is marked by red. Some data from the two observation systems overlap in the range $R \sim$ (0.2 mm, 1 mm), which verifies the consistency of the two systems. At the applied stretch, $\lambda_{appl} = 1.62$, the observed stretch closest to the crack tip is $\lambda_1 = 0.85$ and $\lambda_2 = 3.97$ at the distance $R = 0.01$ mm.

For the pure shear configuration, the height of the sample H is the characteristic length that affects the deformation field. We perform finite element calculation using ABAQUS to study the effect of sample height (Fig. 7). The material is set as an incompressible neo-Hookean solid with its shear modulus $\mu = 5.614$ kPa. The height and width of the model are 10 mm and 50 mm, respectively. The model is simplified as a two-dimensional plane stress state. Due to the symmetry of Mode-I condition, we only include the top half of the pure shear sample in the simulation. The top surface of the model is applied with a displacement u_2, the horizontal displacement is $u_1 = 0$. The bottom surface of the model is divided into two parts with different boundaries. The left part is traction free, and the right part has the vertical displacement $u_2 = 0$. The model is meshed into 77,902 CPS4 elements with the minimum element size being $5*10^{-3}$ mm. The field of energy density W is normalized by the energy density W_0 in the homogeneous deformation region far away from the crack tip. The distance from the crack tip R is normalized by the height of the sample (Fig. 7c). In the region $R/H < 0.1$, the stress concentration prevails and the energy density agrees with the theoretical prediction $W \sim G/R$. When R/H is large, the external boundary prevails and W/W_0 approaches 1. This result indicates that it is expected to find the outer boundary of the G-annulus, $R_2 \sim 0.1H$. Thus, the G-annulus exists in $R_1 < R < 0.1H$. In plotting Fig. 7c, the applied energy release rate, calculated by the J integral, is taken to be the same for different heights H.

As analyzed above, if the inelastic zone R_1 is comparable to $0.1H$, the G-annulus does not even exist and it is difficult to identify the inelastic zone. We prepare hydrogel samples with three different heights, $H = 37$ mm, $H = 20$ mm, $H = 10$ mm (the width/height ratio is fixed as 5:1). For the sample with $H = 10$ mm, the energy release rate at $\lambda_{appl} = 1.62$ is calculated to be 32 J/m^2 by

$$G = HW(\lambda_{appl}) \tag{6}$$

where $W(\lambda_{appl})$ is calculated by integrating the stress-stretch curve of a pure shear sample without crack. The applied stretch 1.62 is very close to the rupture stretch, so that the applied energy release rate 32 J/m^2 is roughly equal to the toughness. For the samples with $H = 20$ mm and $H = 37$ mm, the energy release rate is taken to be the same, 32 J/m^2, which corresponds to the applied stretch $\lambda_{appl} = 1.41$ and $\lambda_{appl} = 1.29$ respectively.

For the three kinds of samples, the energy density as a function of distance from the crack tip $W(R)$ is calculated by Eq. (2) using the observed fields of principal stretches $\lambda_1(R)$, $\lambda_2(R)$, and plotted as red circles in Fig. 8, Fig. 9, Fig. 10. The solid curves in the three figures represent the finite element results for the three geometries under the same energy release rate, 32 J/m^2. The finite element results determine the theoretical prediction $W \sim G/R$ with the proportional coefficient 0.174 (dashed line).

For the samples with different heights, the deviation of the experimental data from $W = 0.174G/R$ identifies the two boundaries of G-annulus. For the sample with $H = 37$ mm, the inner boundary (i.e., the boundary of the inelastic zone) occurs at about $R_1 = 0.7$ mm, while the outer boundary occurs at about $R_2 = 2.5$ mm, which is on the order of $0.1H$ (Fig. 8). For the sample with $H = 20$ mm, the inner boundary occurs at about $R_1 = 0.6$ mm, while the outer boundary occurs at about $R_2 = 1.5$ mm (Fig. 9). For the sample with $H = 10$ mm, we have experimental data observed from both the low-resolution camera (red circles) and the high-resolution microscope (green circles, repeated three times) (Fig. 10). The data very close to the crack tip, observed by the high-resolution microscope, significantly

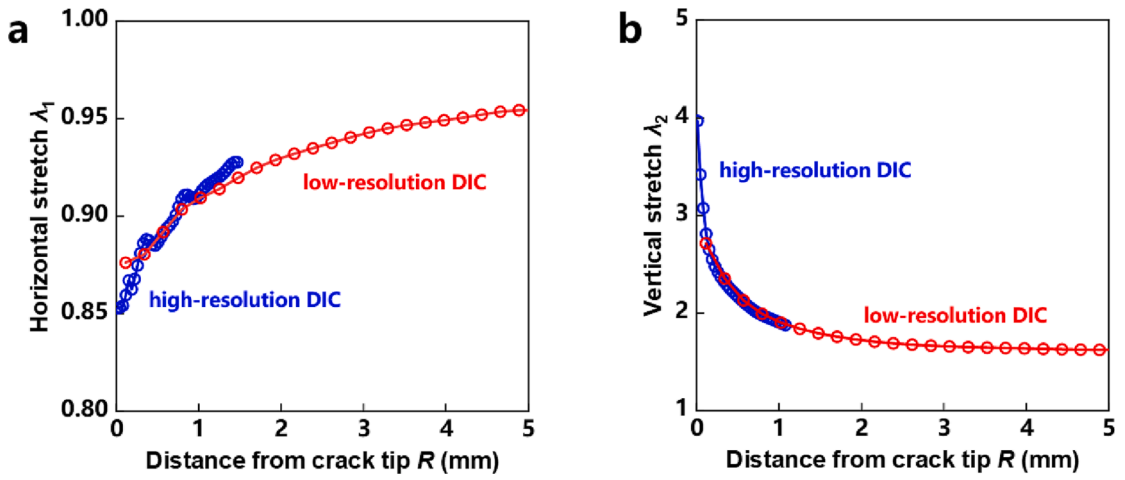

Fig. 6. The observed stretch field. The sample is subject to an applied stretch of $\lambda_{appl} = 1.62$. (a) The principal stretches λ_1 at a distance R ahead of the crack tip. (b) The principal stretches λ_2 at a distance R ahead of the crack tip.

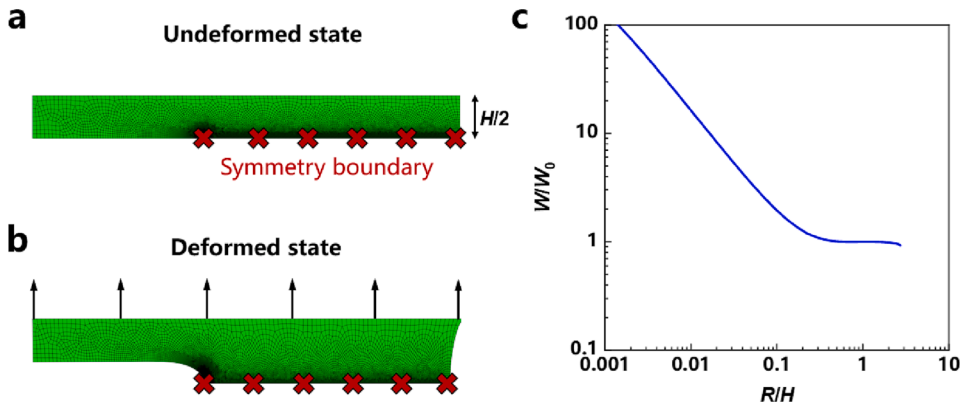

Fig. 7. The crack tip field calculated by finite element method. (a) Undeformed state. (b) Deformed state. The sample is subject to an applied stretch of $\lambda_{appl} = 1.62$. (c) The energy density at distance R ahead of the crack tip, where H is the height of the sample, and W_0 is the energy density of homogeneous deformation.

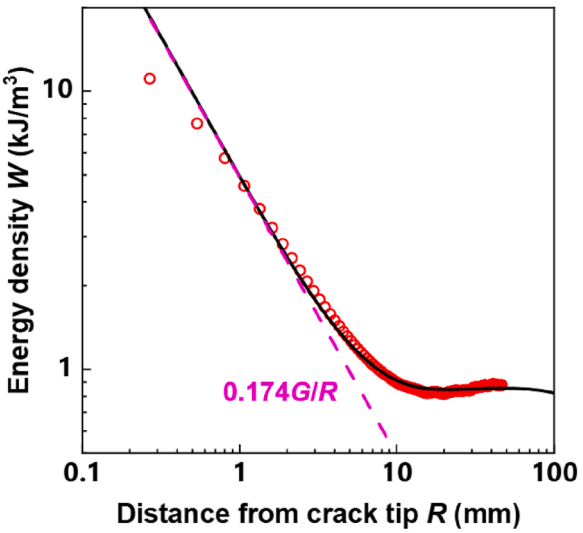

Fig. 8. Energy density at distance R from the crack tip ($H = 37$ mm). A sample of height of $H = 37$ mm is subject to an applied stretch of $\lambda_{appl} = 1.62$. The curve is obtained by the finite element method, and the data points are determined from the low-resolution DIC method.

deviate from the elastic solution $W = 0.174\ G/R$. In this case, the inner boundary occurs at about $R_1 = 0.6$ mm, the outer boundary occurs at about $R_2 = 1$ mm, and the G-annulus is narrow.

Also included in Fig. 10 is the value of work of fracture, $W^* = 51164$ J/m^3, (blue line) integrated by the stress-stretch curve from the uniaxial tensile test (Fig. 3). The trend is that the energy density approaches the work of fracture as the material particle approaches the crack tip. The intersection between the elastic solution $W = 0.174\ G/R$ and the line of constant work of fracture gives a length of $R =$ 0.1 mm. This length is a rough estimation for the inelastic zone, which is a little smaller than $R_1 = 0.6$ mm estimated by the deviation from the elastic solution. This is because the rough estimation assumes the energy density of all the material particles in the inelastic zone is equal to the work of fracture. In fact, before the energy density reaches W^*, the material particles have already undergone inelasticity. The existence of the inelastic zone in the nearly-perfect elastic polyacrylamide hydrogel deserves further study. Possible reasons include the network imperfection [22] and the exchange of water at the crack tip with the environment [23].

The inelastic zone around the crack tip of materials is of general interest. In particular, when the inelastic zone is small compared to the characteristic length scale of the specimen, the measured toughness is a material property, independent of type of the specimen. For metals, the inelastic zone is often identified by the plastic strain after unloading. For soft materials, such as elastomers and hydrogels, plastic strain is often negligible and cannot be used to identify the inelastic zone. Several methods have been proposed to identify inelastic zones in elastomers and gels, but none have been widely practiced [7,8,11]. This paper introduces an approach to identify the inelastic zone of soft materials using the concept of G-annulus. We use digital image correlation to obtain the strain field around the crack tip, calculate the energy density and compare with the theoretical prediction of W ~ G/R. The difference between the measured field and the predicted elastic field identifies the inelastic zone. With this approach, we identify the inelastic zone of an elastic

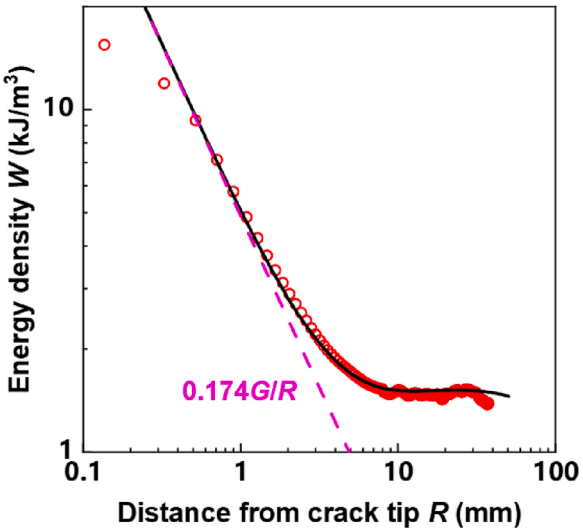

Fig. 9. Energy density at distance R from the crack tip ($H = 20$ mm). A sample of height of $H = 20$ mm is subject to an applied stretch of $\lambda_{\text{appl}} = 1.62$. The curve is obtained by the finite element method, and the data points are determined from the low-resolution DIC method.

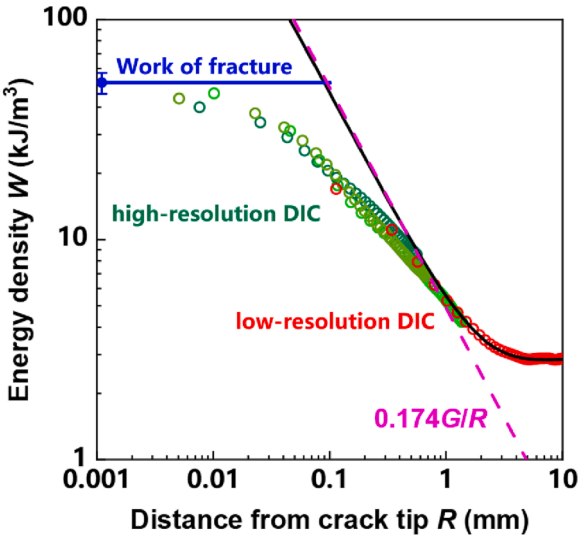

Fig. 10. Energy density at distance R from the crack tip ($H = 10$ mm). A sample of height of $H = 10$ mm is subject to an applied stretch of $\lambda_{\text{appl}} = 1.62$. The curve is obtained by the finite element method, and the data points are determined from both the high-resolution and the low-resolution DIC method.

polyacrylamide hydrogel for the first time, which provides experimental data to help understand the fracture process of polyacrylamide hydrogels. The proposed method may also be used to identify inelastic zones around crack tips in other highly elastic soft materials.

5. Conclusions

In this paper, we use the DIC method to identify the inelastic zone of polyacrylamide hydrogels. We load the hydrogel sample in a pure-shear configuration, and measure the deformation around the crack tip. We use a microscope with the spatial resolution of 2.3 μm/pixel to observe the field very close to the crack tip (0.01 mm ~ 1 mm). We use a camera with the spatial resolution of 22.7 μm/pixel to observe the field on the scale of the sample (0.1 mm ~ 10 mm). The recorded images by both the microscope and the camera are processed by the DIC software and merged into a field that scales from 0.01 mm to 10 mm. The field of energy density W near the crack tip is calculated using the measured strain field, based on the neo-Hookean model and then compared to the theoretical prediction of $W \sim G/R$. The matching region between the experimental data and the theoretical prediction verifies the existence of the G-

annulus. The inner radius of the *G*-annulus indicates the inelastic zone. The outer radius of the *G*-annulus indicates the effect of the sample boundary. The finite element results agree well with the deformation in the *G*-annulus and the external field measured by DIC method.

CRediT authorship contribution statement

Yudong Pan: Writing – review & editing, Writing – original draft, Validation, Software, Methodology, Investigation, Formal analysis, Data curation. **Yifan Zhou:** Conceptualization. **Zhigang Suo:** Writing – review & editing, Supervision, Conceptualization. **Tongqing Lu:** Writing – review & editing, Supervision, Resources, Funding acquisition, Conceptualization.

Declaration of Competing Interest

The authors declare that they have no known competing financial interests or personal relationships that could have appeared to influence the work reported in this paper.

Data availability

Data will be made available on request.

Acknowledgement

TL acknowledges the support of NSFC (No. 11922210). ZS acknowledges the support of NSF MRSEC (DMR-2011754).

References

[1] Liu J, Yang C, Yin T, Wang Z, Qu S, Suo Z, et al. J Mech Phys Solids 2019;133. 103737.
[2] Kim J, Zhang G, Shi M, Suo Z. Fracture, fatigue, and friction of polymers in which entanglements greatly outnumber cross-links. Science 2021;374:212–6.
[3] Hassan S, Kim J. Polyacrylamide hydrogels. IV. Near-perfect elasticity and rate-dependent toughness. J Mech Phys Solids 2022;158:104675.
[4] Lu Y-W, Lupton C, Zhu M-L, Tong J. In situ experimental study of near-tip strain evolution of fatigue cracks. Exp Mech 2015;55:1175–85.
[5] Besel M, Breitbarth E. Advanced analysis of crack tip plastic zone under cyclic loading. Int J Fatigue 2016;93:92–108.
[6] Zhang T, Lin S, Yuk H, Zhao X. Predicting fracture energies and crack-tip fields of soft tough materials. Extreme Mech Lett 2015;4:1–8.
[7] Mzabi S, Berghezan D, Roux S, Hild F, Creton C. A critical local energy release rate criterion for fatigue fracture of elastomers. J Polym Sci B 2011;49:1518–24.
[8] Yu QM, Tanaka Y, Furukawa H, Kurokawa T, Gong JP. Direct observation of damage zone around crack tips in double-network gels. Macromolecules (Print) 2009;42:3852–5.
[9] Smith T, Gupta C, Fan Z, Brust GJ, Vogelsong R, Carr C, et al. Toughness arising from inherent strength of polymers. Extreme Mech Lett 2022;56. 101819.
[10] Sun D, Lu T, Wang T. Nonlinear photoelasticity of rubber-like soft materials: comparison between theory and experiment. Soft Matter 2021;17:4998–5005.
[11] Ducrot E, Chen Y, Bulters M, Sijbesma RP, Creton C. Toughening elastomers with sacrificial bonds and watching them break. Science 2014;344:186–9.
[12] Williams ML. On the stress distribution at the base of a stationary crack; 1957.
[13] Hutchinson J. Singular behaviour at the end of a tensile crack in a hardening material. J Mech Phys Solids 1968;16:13–31.
[14] Rice JR, Rosengren G. Plane strain deformation near a crack tip in a power-law hardening material. J Mech Phys Solids 1968;16:1–12.
[15] Geubelle PH, Knauss WG. Finite strains at the tip of a crack in a sheet of hyperelastic material: II. Special bimaterial cases. J Elast 1994;35:99–137.
[16] Rice JR. A path independent integral and the approximate analysis of strain concentration by notches and cracks; 1968.
[17] Long R, Hui C-Y. Crack tip fields in soft elastic solids subjected to large quasi-static deformation—a review. Extreme Mech Lett 2015;4:131–55.
[18] Long R, Hui C-Y, Gong JP, Bouchbinder E. The fracture of highly deformable soft materials: a tale of two length scales. Annu Rev Condens Matter Phys 2021;12:71–94.
[19] Rivlin R, Thomas AG. Rupture of rubber. I. Characteristic energy for tearing. J Polym Sci. 1953;10:291–318.
[20] Sutton MA, Orteu JJ, Schreier H. Image correlation for shape, motion and deformation measurements: basic concepts, theory and applications. Springer Science & Business Media; 2009.
[21] Bruck H, McNeill S, Sutton MA, Peters W. Digital image correlation using Newton-Raphson method of partial differential correction. Exp Mech 1989;29:261–7.
[22] Yang C, Yin T, Suo Z. Polyacrylamide hydrogels. I. Network imperfection. J Mech Phys Solids. 2019;131:43–55.
[23] Yang Y, Guo H, Du Z, Hong W, Lu T, Wang T. Rate-dependent fracture of hydrogels due to water migration. J Mech Phys Solids 2022;167. 105007.